



**HAL**  
open science

# **Barite and gypsum precipitation in chalk: A numerical simulation approach revealing the coupled impact of physical and chemical heterogeneities in porous media**

A. Rajyaguru, Nicolas Seigneur, O. Bildstein, S. Savoye, Charles Wittebroodt, E.L. Hôpital, V. Detilleux, P. Arnoux, Vincent Lagneau

## **► To cite this version:**

A. Rajyaguru, Nicolas Seigneur, O. Bildstein, S. Savoye, Charles Wittebroodt, et al.. Barite and gypsum precipitation in chalk: A numerical simulation approach revealing the coupled impact of physical and chemical heterogeneities in porous media. *Chemical Geology*, 2022, 609, pp.121069. <10.1016/j.chemgeo.2022.121069>. <hal-03758342>

**HAL Id: hal-03758342**

**<https://minesparis-psl.hal.science/hal-03758342v1>**

Submitted on 2 Sep 2024

HAL is a multi-disciplinary open access archive for the deposit and dissemination of scientific research documents, whether they are published or not. The documents may come from teaching and research institutions in France or abroad, or from public or private research centers.

L'archive ouverte pluridisciplinaire HAL, est destinée au dépôt et à la diffusion de documents scientifiques de niveau recherche, publiés ou non, émanant des établissements d'enseignement et de recherche français ou étrangers, des laboratoires publics ou privés.



Distributed under a Creative Commons CC BY-NC-ND 4.0 - Attribution - Non-commercial use - No Derivative Works - International License

1 *Barite and gypsum precipitation in chalk: A numerical simulation approach revealing*  
2 *the coupled nature impact of physical and chemical heterogeneities in porous media*

3

4 **Authors:**

5 *A. Rajyaguru<sup>1,2\*</sup>, N. Seigneur<sup>2</sup>, O.Bildstein<sup>3</sup>, S.Savoye<sup>1</sup>, C. Wittebroodt<sup>4</sup>, E. L. 'HÔPITAL<sup>4</sup>, V.*

6

*Detilleux<sup>5</sup>, P.Arnoux<sup>1</sup>, V. Lagneau<sup>2</sup>*

7

8 *(1) Université Paris-Saclay, CEA, Service d'Etude du Comportement des Radionucléides*

9

*(SECR), , Gif-sur-Yvette*

10

*(2) Centre de Géosciences, MINES ParisTech, PSL Research University, Paris, France*

11

*(3) CEA, DES, IRESNE, DTN, Laboratory for Modeling of Transfers in the Environment,*

12

*Saint Paul-lez-Durance, France*

13

*(4) IRSN, LETIS, Fontenay Aux Roses, France*

14

*(5) Bel V, Belgium*

15

16

17

18

*Corresponding author address: [ashish.rajyaguru@psi.ch](mailto:ashish.rajyaguru@psi.ch)*

19

# Abstract

20

21 In studies relevant to contaminant transport in geosphere, evolution of local physicochemical  
22 processes imparts potential challenges in safety and critical assessment issues. The  
23 transport of such contaminants in a rock pore structure could occur under advective or  
24 diffusive regime. Such transport over spatial and temporal scale depends upon coupling  
25 between physical properties of pore structure (permeability, pore size distribution, porosity)  
26 and chemical properties of dissolved ionic species (pH, ionic strength, and surface  
27 interactions). The nature of such interactions leads to generation of local imbalances in pore  
28 solution and enhances dissolution and precipitation of minerals. To predict occurrence of  
29 such processes over large spatial and temporal scales, it is imperative to demonstrate how  
30 the physical and chemical processes interact within the heterogeneous porous media. In this  
31 context, numerical simulations were conducted to model the results of experimental dataset  
32 investigating barite and gypsum precipitation in chalk. In the experimental approach, the  
33 selected two minerals are end-members of the sulfate-alkali family and exhibit large  
34 differences in kinetic rate and solubility, and the reference chalk sample resembles  
35 heterogeneity in its pore structure. The numerical simulations revealed that at 1D scale, it  
36 was possible to model overall experimental observations at boundary monitoring points such  
37 as chemistry evolution in reservoirs, porosity loss during barite and gypsum precipitation,  
38 total amount of barite and gypsum in clogging zone and threshold saturation index to initiate  
39 precipitation. However, these simulations could not validate the experimentally observed  
40 impact of barite and gypsum clogging on changes in water tracer transport. The underlying  
41 reasons for such behavior was the formation of a unique clogging zone due to barite and  
42 gypsum precipitation. We show that 2D simulations incorporating spatial heterogeneity are  
43 able to reproduce the observed precipitation patterns, both for the barite and gypsum  
44 experiments. Through 1D and 2D numerical results, we demonstrate the capability of a  
45 reactive transport model to validate experimentally observed barite and gypsum precipitation  
46 behavior in chalk sample. Furthermore, it also highlights the interplays between  
47 physicochemical heterogeneities, mineral reactivity and transport rates which are  
48 responsible for the precipitation pattern of the precipitates, and hence their impacts on  
49 transport properties.

50

## 51 1 Introduction

52 Contaminant migration in geological formations over large spatial and temporal scales is  
53 mainly governed by reactive transport phenomena. Over time, these contaminants could  
54 interact with rock pore structures and due to their physicochemical nature they could  
55 generate a local imbalance in existing pH and ionic concentration of rock pore solution.  
56 Thus, these local imbalances would result in dissolution of the cemented rock minerals or  
57 formation of secondary mineral species via precipitation phenomena. Indeed, these  
58 secondary processes would modify the existing pore structure and therefore the transport  
59 properties of the rock. For safety and risk analysis, the evolution of such processes over  
60 larger temporal and spatial scales could impose conditions where migration of some  
61 radiotoxic elements is enhanced and with a possibility of their leaking into nearby important  
62 drinking water sources (Moldovan et al., 2003; Thakur et al., 2010).

63 One such study concerning reactive transport in porous media deals with the trapping of  
64 atmospheric CO<sub>2</sub> (global carbon sequestration or GCS) into the rock pore space (Berthe,  
65 2012; Jun et al., 2013; Snæbjörnsdóttir et al., 2020). The sites selected for such concept  
66 contains a porous and permeable rock that could easily trap injected CO<sub>2</sub> within its pore  
67 space. Indeed, a layer of impervious cap-rock that potentially limits any ionic transport into  
68 the surrounding biosphere covers this permeable rock. However, over long term the trapped  
69 CO<sub>2</sub> would gradually interact with the cap-rock and modify its local pore chemistry. These  
70 changes would trigger dissolution and precipitation of halite, sulfate- or carbonate-bearing  
71 minerals that would change cap-rock pore structure and alter its existing sealing properties.  
72 Under such scenario, the transport behavior of some ionic species that are trapped in both  
73 reservoir and sealing rock is altered and a potential risk is generated of their leak into the  
74 surrounding biosphere. Similarly, such secondary process over long times scales could also  
75 occur in deep geological host facilities capable for confining long-lived intermediate and  
76 high-level radioactive waste (Bradbury et al., 2014). For example, the degradation of cement  
77 structures, corrosion of steel assemblies and release of ionic species as fission products  
78 would result in generation of chemically active saline or alkaline plumes. Similar to CO<sub>2</sub>  
79 sequestration sites, these plumes could interact with cap rock and modify its intact transport  
80 properties. In this case, it could leak radiotoxic ions into surrounding biosphere and generate  
81 safety issues. Thus, to evaluate the long-term durability of deep geological disposal sites, it  
82 is imperative to obtain a robust understanding of the occurrence of such physicochemical  
83 processes and their impact on the properties of host rock as well as sealing rock over larger  
84 temporal and spatial scales.

85 Over the years, the understanding of solute transport in geosphere is built upon lab-scale or  
86 field scale experimental observations, combined with numerical simulations using  
87 geochemical models based on a continuum approach (Bear, 2013; Glaus et al., 2020;  
88 Lagneau, 2013; Landesman et al., 2018; Seigneur et al., 2019). The advantage of using  
89 such numerical models lies on the representation of the volume of interest as representative  
90 elementary volumes (REV) that characterize the local properties of the material such as  
91 porosity, diffusivity, permeability, etc. Using this assumption it is possible to simplify the  
92 natural but complex geometry of the material at 1D or 2D (homogenized) and to simulate its  
93 evolution on large time and space scales. In such models, minerals constituting a selected  
94 natural porous material are described in volume fractions and total porosity is the void space  
95 between these minerals. A multicomponent reactive fluid containing selected ions of interest  
96 is allowed to migrate through these void spaces. From experimental observations, one could

97 now fix the initial and boundary conditions in the numerical simulations and observe the  
98 evolution of dominant physicochemical processes on selected spatial and temporal scale. In  
99 this model the dominant processes such as mineral dissolution or precipitation are modeled  
100 via classical kinetic rate law in which key input parameters such as kinetic rate constant,  
101 saturation index, reactive surface area are obtained from existing thermodynamic database  
102 in literature (Lasaga, 2014). Finally, the formation of new void spaces and their feedback on  
103 transport properties (permeability, local porosity, diffusivity) are modeled using empirical  
104 relationships such as Kozeny-Carman and Archie's relationships (Archie, 1942; Carman,  
105 1937). However, recent studies have shown that formation of secondary mineral is  
106 dependent on local pore chemistry and plays an important role in development of overall  
107 clogging zone and thereby changes on overall rock transport properties (Sabo and  
108 Beckingham, 2021; Seigneur et al., 2019; Steinwinder and Beckingham, 2019).

109109

110 Thus, replacement of such empirical relationships is complex because rock pore matrix  
111 contains multiscale physical and chemical properties such as pore size distributions, surface  
112 charge, surface roughness, reactive/non-reactive phases, local precipitation/dissolution rate,  
113 pore pressure effect, and varying mineral solubility. In reality, rocks or porous soils may  
114 contain such physicochemical spatial properties from micron-size pore scale to submillimeter  
115 scale to the basin scale and their coupling further control the interplay between mass  
116 transport and reaction kinetics, creating altered zones favoring precipitation/dissolution(  
117 Berkowitz et al., 2006; Bruns et al., 2017; Noiriél et al., 2021; Trincheró and Iraola, 2020).  
118 Thus, it is imperative to investigate local reaction kinetics and the corresponding mass  
119 transport changes at pore scale for diverse range of porous materials and minerals relevant  
120 of geochemistry for the development of new feedback relationships that could replace the  
121 existing Archie's or Kozeny-Carman relationships (Nooraiepour et al., 2021; Steefel and  
122 Yang, 2021; Varzina et al., 2020).

123 In this view, the aim of this study is to investigate numerically the impact of mineral intrinsic  
124 properties (solubility, precipitation rate, nucleation driven growth) on secondary mineral  
125 formation and the corresponding feedback on transport properties of reference porous  
126 media. The numerical simulations presented in this study are based upon experimental  
127 dataset that investigated barite and gypsum precipitation in natural chalk sample (Rajyaguru  
128 et al., 2019). The experimental dataset were obtained based on the following principle, "fix a  
129 physical property namely pore structure heterogeneity using chalk sample and combine it  
130 with chemical property using two extremities (solubility and rate of precipitation) of sulfate  
131 alkali minerals." From this principle, it was possible to investigate the coupling effect of both  
132 properties on governing distributions of barite and gypsum mineral in the precipitation zone  
133 as well as their impact on the existing transport properties of chalk sample. The first  
134 experiment showed that barite precipitation resulted in the formation of a thin-layered  
135 clogged zone located in center of chalk sample. On the contrary, the second experiment  
136 showed that gypsum precipitation resulted in formation of isolated clusters type of clogged  
137 zone at the center of chalk sample. The water tracer tests conducted prior and after clogging  
138 phenomena showed that both of these distributions had contrasting impact on changes in  
139 chalk transport properties (with barite imparting significant reduction in tracer diffusivity  
140 compared to gypsum).

141 Thus, numerical description of these experimental results required a two-step approach. In  
142 the first step, using the initial and boundary conditions from experiments, barite and gypsum  
143 precipitation simulations were carried out in a homogeneous 1D geometry with total porosity  
144 of 45% (representing the mean porosity of chalk sample). The aim of these simulations was  
145 to determine the time at which precipitation is initiated, the resulting width of clogged zone  
146 and subsequent porosity reduction, and finally the evolution of chemistry evolution in  
147 reservoirs when precipitates formation modifies the pore structure of chalk sample. Indeed,  
148 at 1D, the feedback of clogged zone formation on tracers transport was simulated using  
149 empirical Archie's relationship. However, one must note that 1D simulations do not integrate  
150 spatial variability in pore size distribution of chalk sample. Thus in the second step, 2D  
151 simulations were required to accommodate this property, where pore size distribution of  
152 chalk was mimicked by integrating variable porosity ( $45\% \pm 5\%$ ) while keeping the initial  
153 boundary and chemical conditions same as of 1D simulations. Since, one cannot fully  
154 resolve Archie's relationship in 2D (Deng et al., 2021), the objective of the simulations in this  
155 step was to investigate underlying factors controlling changes in distributions of barite and  
156 gypsum minerals.

157157

## 158 2 Numerical methods

### 159 2.1 Governing equations for numerical modeling

160 The generalized equation for modeling at REV-scale in HYTEC is well described  
161 in(Cochepin et al., 2008; Lagneau, 2013; Lagneau and van der Lee, 2010). The kinetic rate  
162 equation to model experimentally observed barite or gypsum reacted zones in chalk is  
163 described in equation-1.

$$r_s = -A_{bulk}k_{rate} \left[1 - \left(\frac{Q_s}{K}\right)\right] \quad (1)$$

164 where,  $Q_s$ : ion activity product, and  $K$ : mineral equilibrium constant. The bulk surface area  
165  $A_{bulk}$  represents the overall surface over which precipitation can occur. It is the combination  
166 of the precipitation over the existing pore walls as well as a growth on barite/gypsum nuclei.  
167 These bulk surface areas can be derived from the specific surface area  $A_s$  using Equation-2

$$A_{bulk}(m^2 \cdot m^{-3}_{solution}) = A_{s,pm}C_{pm} + A_{s,min}C_{min} \quad (2)$$

168168

or 
$$A_s = 3/\rho r \quad (3)$$

169 where,  $\rho$ : particle density,  $r$ : radius of spherical particle,  $C$ : Particle concentration (g/L).  
170 Hence, an initial reactivity of the porous medium is described using an unreactive mineral,  
171 with an uniform concentration ( $C_{pm}=1\text{g/L}$ ) and a specific surface area of  $A_{s,pm} = 1 \text{ m}^2/\text{g}$ , in line  
172 with literature data(Hjuler and Fabricius, 2009; Røgen and Fabricius, 2002). Then, reactivity  
173 evolves as precipitation proceeds and provides an increasing value for the bulk surface area  
174 due to evolution of  $C_{min}$ . This description is similar to the one used by (Noiriel et al., 2021).

175 The feedback impact of clogging on diffusivity is modeled using modified Archie's law as  
176 represented in equation 4(van der Lee et al., 2003)

$$D_e(\omega) = D_e(\phi_0) \left(\frac{\phi - \phi_c}{\phi_0 - \phi_c}\right)^\alpha \quad (4)$$

177 where  $D_e$ : effective diffusion coefficient,  $\phi_c$ : percolation threshold,  $\alpha$ : cementation factor

## 178 2.2 Numerical Modeling

### 179 2.2.1 1D simulations to model reacted zone

180 The 1D simulations were carried out to mimic counter diffusion setup used in the  
181 experiments of (Rajyaguru et al., 2019). The geometry consists of two 1 mm reservoirs  
182 sandwiching a chalk sample of uniform porosity 45% and thickness of 6.7 mm. In the  
183 experiments, the actual reservoir volumes were 178 ml for  $\text{BaCl}_2/\text{CaCl}_2$  reservoirs and  
184 138 ml for  $\text{Na}_2\text{SO}_4$  reservoirs. In numerical, inserting such large volumes at boundary would  
185 result very large simulation time Thus, a bypass technique is used where 1 mm numerical  
186 reservoirs are created with porosities equal to 187 for  $\text{Ca}^{2+}/\text{Ba}^{2+}$  reservoir and 145 for  $\text{SO}_4^{2-}$   
187 reservoir. This trick yields the correct volume (and contents in solutes) while maintaining a  
188 short distance and maximizing diffusion between the reservoirs and the chalk sample. The  
189 sample in 1D simulations was discretized with  $dx = 100 \mu\text{m}$ . To initiate the counter diffusion,  
190 the initial chemical conditions in each reservoirs were derived from experimental conditions  
191 (**Table-S1 in Supporting information**). The modeling process starts by allowing these ionic  
192 species to counter diffuse and meet in the sample pore space. Over time, these ions locally  
193 increase supersaturation in pore solution with respect to barite or gypsum. Experimentally,  
194 the supersaturation state required to initiate precipitation is 4.0 for barite (Prasianakis et al.,

2017) and 0.3 for gypsum. Over time, the precipitation initiation only takes places in points that achieved this supersaturation threshold (Kashchiev and van Rosmalen, 2003; Prieto, 2014), for which Equation (1) is used. In HYTEC, initiation of first precipitates is achieved using a kinetic rate law that represents homogeneous nucleation in the entire sample by spraying the system with a pseudo-mineral “nucleus” (concentration  $C_{pm}$ ) of low reactive surface area ( $A_{s,pm}$ ). Once the supersaturation in first line of precipitation is achieved, the nucleus will allow initiation of selected mineral precipitation. Nevertheless, at the beginning of experiment if a mineral is present in a system then precipitation will occur (possibly under kinetic control) as soon a saturation is reached (saturation index  $\geq 0$ ). The values of the kinetic rate constant ( $k_{rate}$  in  $\text{mol m}^{-2} \text{s}^{-1}$ ) and specific surface area ( $A_{s,min}$  in  $\text{m}^2 \text{g}^{-1}$ ) for barite and gypsum equal to  $k_{rate\_barite} = 1 \times 10^{-11}$ ;  $k_{rate\_gypsum} = 1.5 \times 10^{-6}$  and  $A_{s\_barite} = 0.32$  and  $A_{s\_gypsum} = 1.65$  were initially derived from literature (Nagaraja et al., 2007; Potgieter and Strydom, 1996; Zhang and Nancollas, 1992). During simulations, these base values were slightly calibrated to improve the match with experimental results. In the experimental results, the diffusion behavior of ionic species from respective reservoirs into the sample were measured by periodic concentration acquisition from beginning until 140<sup>th</sup> day of experimental time. Similar concentration curves were obtained via 1D simulations and were compared with experimental results to obtain an insight on how diffusion behavior of each species changes in response to evolving precipitation in chalk sample. Similarly, tracer tests were modeled from 0 to 70 days and 70 to 140 days to estimate the precipitation feedback on chalk transport properties at different times. This feedback effect in 1D simulations were modeled using equation-4.

Sensitivity analyses were carried out to test the impact of, (1) the mesh size, by decreasing it from 100  $\mu\text{m}$ , to 50 and 25  $\mu\text{m}$ , (2) the cementation factor on evolution of reacted zone, with values varying from 1.5 to 2.1 and (3) the supersaturation values used to initiate the gypsum or barite precipitations. The results of each sensitivity test are presented in **Supporting Information**.

222222

### 223 2.2.2 2D simulations

224224

In these simulations, the initial concentration conditions of reactants in respective reservoirs and boundary conditions were kept identical as 1D simulations. However, the system in y-direction is increased up to 8 mm high with discretization as 100  $\mu\text{m}$  along x- and y-axis. Similar to the 1D simulations, the reservoirs are described with porosity greater than one, to account for a larger volume, without having to resort to a too high number of nodes.

As noted in previous section, the 1D base simulations for both barite and gypsum case were modeled using a homogeneous porosity distribution in chalk sample. The kinetic rate equation used to model evolution of reacted zone uses saturation indexes that purely depend upon thermodynamic solubilities derived for bulk systems. As explained in the introduction section, the aim of this study is to demonstrate the combined effect of pore geometry (pore-scale diffusion, pore pressure, reactive surface area) and mineral intrinsic properties (solubility, precipitation rate, nucleation driven growth). However, to quantify each of these parameters one needs quantified dataset explaining local dynamics of precipitates formation, nucleation kinetics and detailed pore size distribution (Rajyaguru et al., 2019).

239 However, the choice of experimental setup and measurements techniques posed restriction  
240 on obtaining such local dynamic processes. Moreover, experimental observations have  
241 clearly shown a two-dimensional regime of precipitation, which cannot be represented by 1D  
242 simulations. Thus, 2D simulations were carried out and the end-results are compared with  
243 micro-tomographic images of clogged area formed by barite and gypsum in chalk samples.  
244 The aim of such comparison was to explain quantitatively the underlying processes  
245 governing global distribution of precipitates in the clogging area. To obtain a broader  
246 understanding of such underlying processes, simulations were performed using different  
247 approaches. First, 2D simulations were performed by using a non-uniform reactivity of the  
248 porous medium to account for varying reactive surfaces initially present in chalk sample and  
249 their impact on governing distributions of barite and gypsum in clogging area (non-uniform  
250 distribution of  $C_{pm}$ ). Then, heterogeneous distribution of porosities was considered to  
251 describe impact of local variation in diffusion of ionic species. Two cases were considered: a  
252 initial purely random Gaussian heterogeneous porosity field (Fig. 1a) and a structured  
253 heterogeneous porosity field (Fig. 1b). Third, different kinetic scenarios were investigated to  
254 disentangle the nucleus-driven nucleation vs a crystal-growth nucleation (Table 1). A direct  
255 comparison of barite and gypsum distributions in latter case allowed us to derive the porosity  
256 field that closely mimicked pore structure of natural chalk used in the experimental study of  
257 (Rajyaguru et al., 2019). Finally, comparing results of both cases with experimental  
258 observations allowed us to demonstrate whether pore structure heterogeneity controlled  
259 transport local ionic species diffusion or generating varying reactive surface was responsible  
260 for distinct distribution of gypsum and barite in the chalk sample.

261 Figure-1 shows two representative porosity fields accounting for purely random  
262 heterogeneity and structured heterogeneity. As shown in Figure1A, the first random porosity  
263 field was generated without spatial structure with a normal distribution centered on 0.45, with  
264 a standard deviation 0.05. The end results of simulations obtained using such random  
265 heterogeneous porosity field provide us a good starting point to inspect as whether initial  
266 presence of surface sites reactivity or pore structure heterogeneity had a pronounced impact  
267 on controlling distributions of barite and gypsum in chalk sample. However, one must note  
268 that the pore structure of natural chalk sample is formed via breaking down of algae known  
269 as coccolithophore into calcite grains. Depending upon the burial depth, the heterogeneity of  
270 pore structure in chalk sample consists of macropores stemming from coccolithophores and  
271 microporosity between void spaces of calcite grains. Several studies focusing on  
272 petrophysics of natural chalk have shown that such heterogeneities could be decomposed  
273 into statistically representative elementary volumes (SREV<sup>s</sup>) of correlation lengths ranging  
274 from 5  $\mu\text{m}$  to 100  $\mu\text{m}$  (Bruns et al., 2017; Müter et al., 2014; Villanova et al., 2013).  
275 Nevertheless, as formation of chalk pore structure purely depends on the nature of  
276 sedimentation process and burial depth, these correlation lengths of SREV<sup>s</sup> could  
277 significantly vary for same family of micritic chalk at different burial sites (Faÿ-Gomord et al.,  
278 2017; Yoon and Dewers, 2013). In the present study, such correlation lengths could be used  
279 to demonstrate if representation of a REV in form of such structured heterogeneities could  
280 result in closer prediction of barite and gypsum distributions in chalk samples. In this view, a  
281 second random porosity field shown in Figure-1B was generated with the same mean and  
282 deviation as purely random case, but integrating a spatial structure with a correlation length  
283 of 100  $\mu\text{m}$ ; the porosity field was simulated using the geostatistics library RGeostats (Renard  
284 et al., 2015). For both cases, the counter diffusion geometry, initial Ca/Ba and  $\text{SO}_4$  reservoir

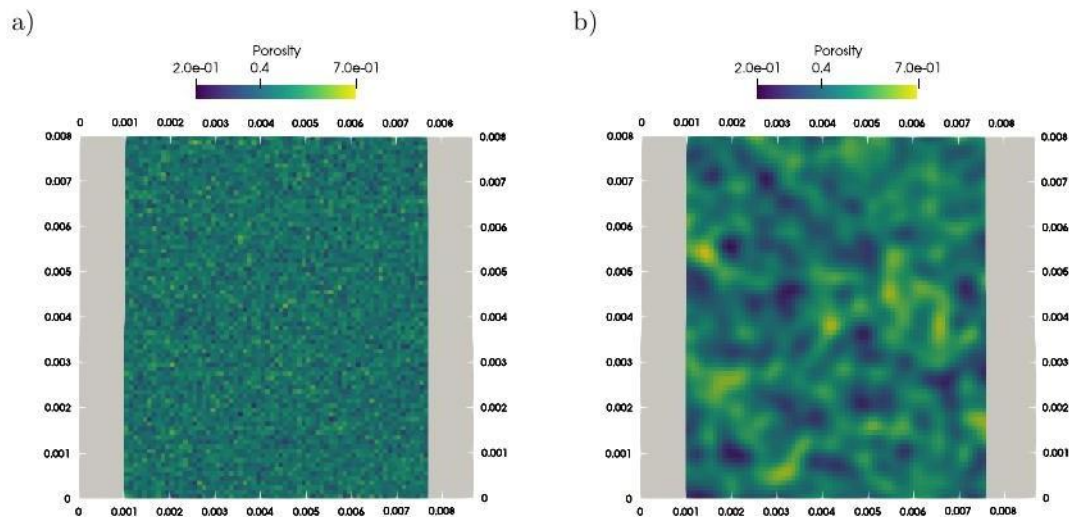
285 concentrations, diffusive coefficients, kinetic rate constants and specific surface area were  
286 kept similar to 1D simulations.

287287

288 Table 1: Input parameters for kinetic rate expressions: chalk reactivity ( $A_{s,pm}$  in  $m^2.g^{-1}$ ), and mineral  
289 surface area ( $A_{gypsum}$  and  $A_{barite}$  in  $m^2.g^{-1}$ ) and supersaturation ( $SI$ ) used for gypsum and barite growth  
290 in subset nucleus driven and transport driven growth.

Case	$a_{s,pm}$	$A_{s,Gypsum}$	$SI_{GYPSUM}$	$A_{s,Barite}$	$SI_{barite}$	
Nucleus driven growth	1	0.1	0.3	1.8		4
Nucleus driven growth	100	0.1	0.3	1.8		4
Transport driven growth	1	10	0.3	1.8		4

291291



292292

293 Figure 1: Random porosity fields used in the 2D simulations. A: purely random unstructured gaussian  
 294 porosity field with mean 45% and std 5%. B: random gaussian porosity field with a correlation length  
 295 of 100  $\mu\text{m}$ .

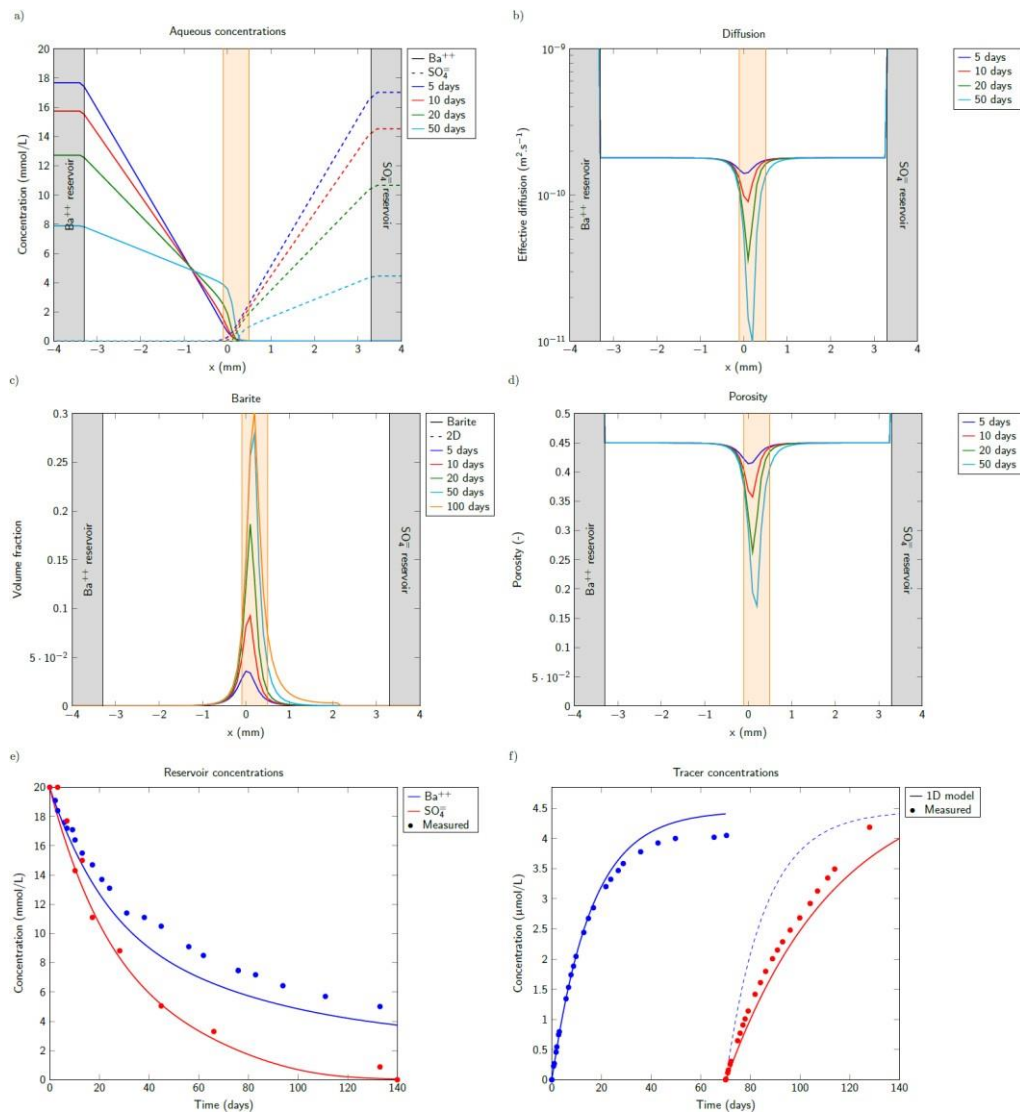
296296

## 297 3 Results and discussion

### 298 3.1 Barite Base Simulation

299 The 1D simulation results for barite precipitation and its feedback impact on tracer diffusivity  
 300 are presented in Figure 2 with a comparison to experimental results from (Rajyaguru et al.,  
 301 2019). As the simulation starts, the reactants diffuse into the chalk sample and decrease the  
 302 ionic concentrations in the reservoir (Figure 2e). Consequently, Figure 2a shows a simulated  
 303 diffusion profile for  $\text{Ba}^{2+}$  and  $\text{SO}_4^{2-}$  from each side of chalk surface towards the center of the  
 304 sample. Over the simulation time,  $\text{Ba}^{2+}$  and  $\text{SO}_4^{2-}$  ions meet in the center of the chalk sample  
 305 and increase the saturation of pore solution with respect to barite mineral. Once the  
 306 threshold super-saturation is achieved, barite precipitates locally. Owing to the very low  
 307 solubility product for barite, the simulations show that barium and sulfate concentrations are  
 308 kept very low within the precipitation zone. The simulations further show that most of the  
 309 barite precipitates grow in this first line of precipitation and the resulting clogging front  
 310 evolves in a thin zone (Figure 2c). A progressive porosity loss and consequent diffusivity  
 311 decrease (Figure 2b and 2d, resp.) is evidenced in this clogging zone. Indeed, as the size of  
 312 clogging zone starts to become significant, a clear feedback on porosity and diffusivity loss is  
 313 observed on  $\text{Ba}^{2+}$  and  $\text{SO}_4^{2-}$  concentration profiles in the reservoir (Figure 2a). After 50 days,  
 314 the diffusive barrier created by the barite layer isolates the two reservoirs, consequently  
 315 limiting any further precipitation process. This was observed experimentally with barium  
 316 concentration reaching quasi-equilibrium state (Figure 2e). At this stage, using the initial and  
 317 final concentration, it is possible to estimate the contribution of  $\text{Ba}^{2+}$  to barite precipitation in  
 318 chalk sample. The simulations predicted that 2.7 mol of Barite precipitated in chalk sample.  
 319 This estimate was well in accordance with experimental estimated barium contribution to  
 320 barite precipitation, *i.e.* 2.5 mol “for detailed calculation refer to (Rajyaguru et al., 2019)”. At  
 321 the end of the simulations, the predicted final thickness of clogging zone (highlighted in

322 orange in Figure 2f) is equal to  $\sim 600 \mu\text{m}$  (which is close to  $\sim 500 \mu\text{m}$  barite zone in chalk  
 323 sample observed by BSE-SEM images in (Rajyaguru et al., 2019)). To estimate the  
 324 feedback of barite precipitation on diffusion, water tracer tests performed at 0 days and 70  
 325 days after the start of the clogging experiment. However, Figure 2f shows that the numerical  
 326 simulations slightly underestimated the reduction in tracer profile for the case of 0 to 70 days  
 327 and slightly overestimated the reduction in tracer profile for 70 to 140 days. This small  
 328 contradiction between experimental and numerical results is due to the fact that in real  
 329 sample the impact on tracer transport occurred due to the occurrence of clogging  
 330 phenomena in a 3D-heterogeneous pore structure, whereas the numerical simulations  
 331 calculated the tracer profiles based upon the total porosity loss at 1D using Archie's  
 332 relationship. One must note that the results presented in supporting information for  
 333 sensitivity of mesh size and cementation factor reveals a limited impact of these parameters  
 334 on the final outcomes of 1D simulations. Conversely, kinetic rate and chalk initial reactive  
 335 surface area exhibit a larger control on simulation results.



336336

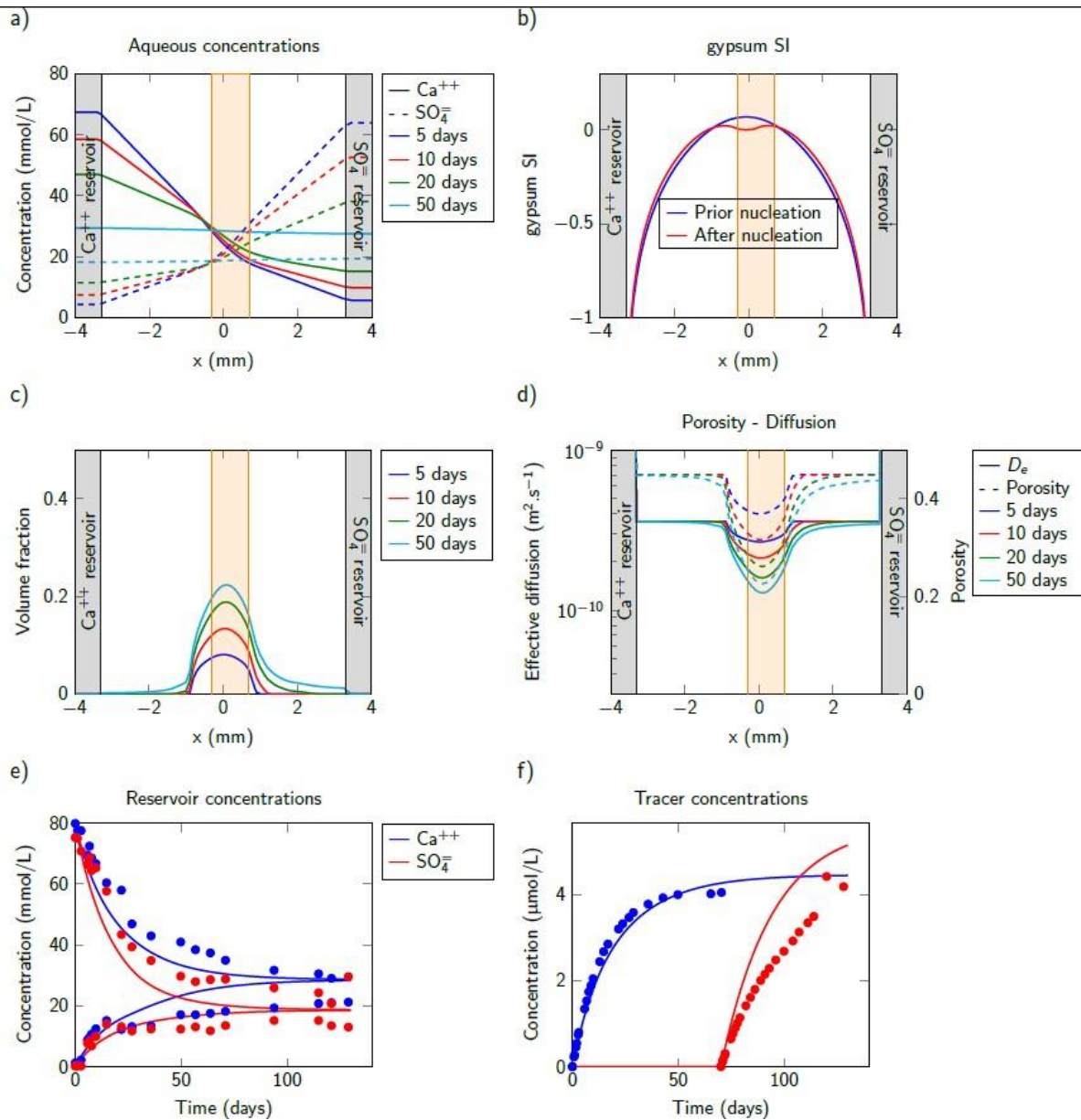
337 Figure 2: comparison between HYTEC and experimental data for chalk barite simulation. **A:**  
 338 concentration profiles for  $\text{Ba}^{2+}$  and  $\text{SO}_4^{2-}$  at 5, 10, 20 and 50 days, **B:** evolution of the effective

339 diffusion coefficient, **C**: barite volume fraction profiles, **D**: evolution of porosity **E**: Evolution of  
340 reservoir concentrations for  $\text{Ba}^{2+}$  and  $\text{SO}_4^{2-}$  and comparison between models (1D & 2D) with measured  
341 values (circles), **F**: Experimental (circles) and numerical (continuous line) water tracer evolution in  
342 downstream reservoirs for water tracer injected at 0 days and 70 days after barite precipitation. One  
343 must note that the dashed line represents a translation of the initial blue model line, and orange zone  
344 represents central zone of the chalk sample.

## 345 3.2 Gypsum Base Simulation

### 346 3.2.1 1D simulation

347 Figure 3, represents the 1D numerical results for gypsum precipitation in chalk sample. The  
348 simulations show that as  $\text{Ca}^{2+}$  and  $\text{SO}_4^{2-}$  diffuse into the chalk sample, a progressive  
349 increase in the saturation with respect to gypsum is observed in the center of the sample  
350 (figure 3b). The concentration profiles of  $\text{Ca}^{2+}$  and  $\text{SO}_4^{2-}$  (Figure 3a & 3e) show that each of  
351 the ion diffuses from their respective reservoirs into the chalk sample and then into the  
352 counter reservoir. These figures show an increase in  $\text{Ca}^{2+}$  and  $\text{SO}_4^{2-}$  concentration in  
353 counter reservoirs for initial 20 days, after which their concentration reach a quasi-  
354 equilibrium state for 140 days of experimental time. Such increase in their concentration  
355 resulted in small precipitation of gypsum in both reservoirs. The numerical simulations were  
356 able to reproduce these experimentally observed concentration profiles and hinted towards  
357 gypsum precipitation in reservoirs (Figure 3c). This is marked by the discontinuity in the  
358 reservoir concentration curves (Figure 3e), which occurs when supersaturation to initiate  
359 precipitation is reached in the reservoir. As a result, their diffusion profiles are very different  
360 compared to the barite case (compare Figure 3a to Figure 2a). Unlike barite, gypsum is a  
361 fairly soluble mineral, so that the pore solution requires more calcium and sulfate ions to  
362 reach the saturation threshold to initiate precipitation. Consequently, longer times are  
363 required to achieve such saturation values that could initiate precipitation and form a strong  
364 clogging zone capable of restricting the diffusion  $\text{Ca}^{2+}$  and  $\text{SO}_4^{2-}$  ions into the counter  
365 reservoir. However, once the precipitation starts a progressive increase of gypsum mineral in  
366 the chalk sample takes place (Figure 3c). Similar to barite case, the impact of gypsum  
367 precipitation on chalk sample was estimated by tracer tests performed at 0 days and 70 days  
368 and 70 to 140 days after the start of the clogging experiment. The corresponding numerical  
369 results presented in Figure 3f shows that the numerical simulations reproduced the tracer  
370 profile for the case of 0 to 70 days, but clearly underestimated the tracer profile for 70 to 140  
371 days. This limitation of 1D simulations to describe the impact of gypsum clogging on chalk  
372 transport properties clearly suggests that small-scale heterogeneity either in reactive surface  
373 area or in transport properties is likely to have a pronounced impact on distribution of  
374 precipitates, width of the clogging area and feedback on tracer diffusivity. Indeed, a direct  
375 comparison between Figure 3c and Figure 2c shows that even at 1D scale the final width of  
376 clogging zone is strongly dependent on the ratios between, solubility, precipitation kinetics  
377 and transport properties. Thus, to describe properly the barite and gypsum clogging in chalk  
378 samples it is imperative to perform numerical simulation with similar initial and boundary  
379 conditions as 1D scale but now taking into account the pore scale heterogeneities. For such  
380 approach, one needs to move from 1D scale to 2D scale.



381

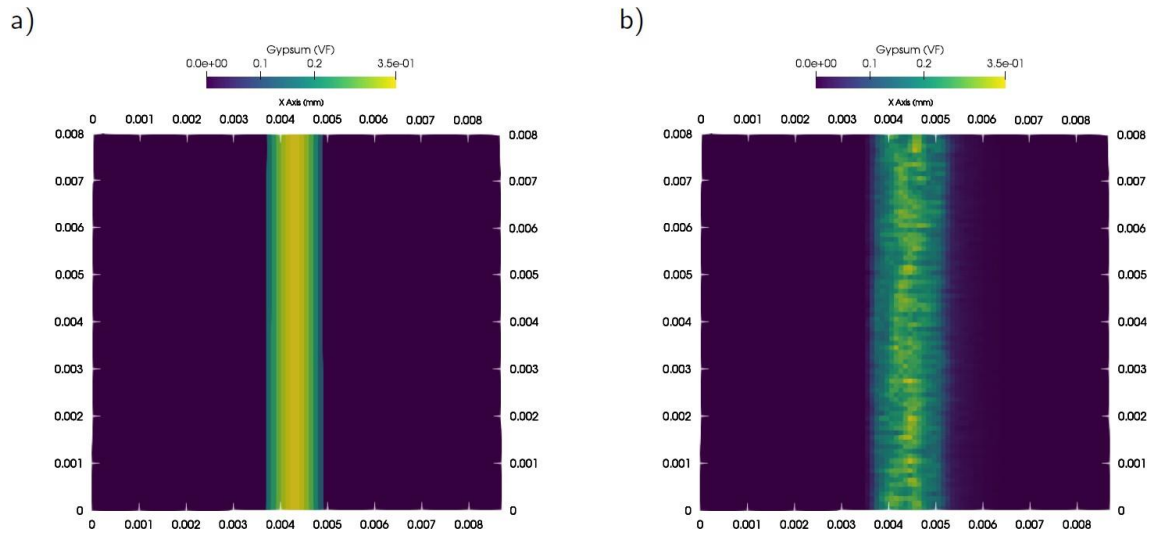
382 Figure 3: comparison between HYTEC and experimental data for basic chalk gypsum simulation, A:  
 383 Concentration profiles of  $\text{Ca}^{2+}$  (solid lines) and  $\text{SO}_4^{2-}$  (dashed lines) **B**: gypsum saturation index at 5,  
 384 10, 20 and 50 days in the precipitation zone, **C**: gypsum volume fraction profile in the sample and in  
 385 the reservoirs, **D**: porosity loss due to gypsum precipitation and its impact on local diffusivity  
 386 reduction in the center of the sample, **E**: Experimental (circles) and numerical (continuous line)  
 387 concentration evolution of  $\text{SO}_4^{2-}$  and  $\text{Ca}^{2+}$  in their respective reservoirs for total experimental time of  
 388 140 days, **F**: Experimental (circles) and numerical (continuous line) water tracer evolution in  
 389 downstream reservoirs for water tracer injected at 0 days and 70 days after gypsum precipitation. One  
 390 must note that the orange zone represents central zone of the chalk sample where most of the clogging  
 391 occurred during precipitation process.

392

### 393 3.2.2 2D simulations

394 At first, gypsum simulations were performed using a varying reactivity of the porous medium  
 395 within the chalk sample (Fig 4a) and using a purely random porosity field (Fig 4b). Fig 4a

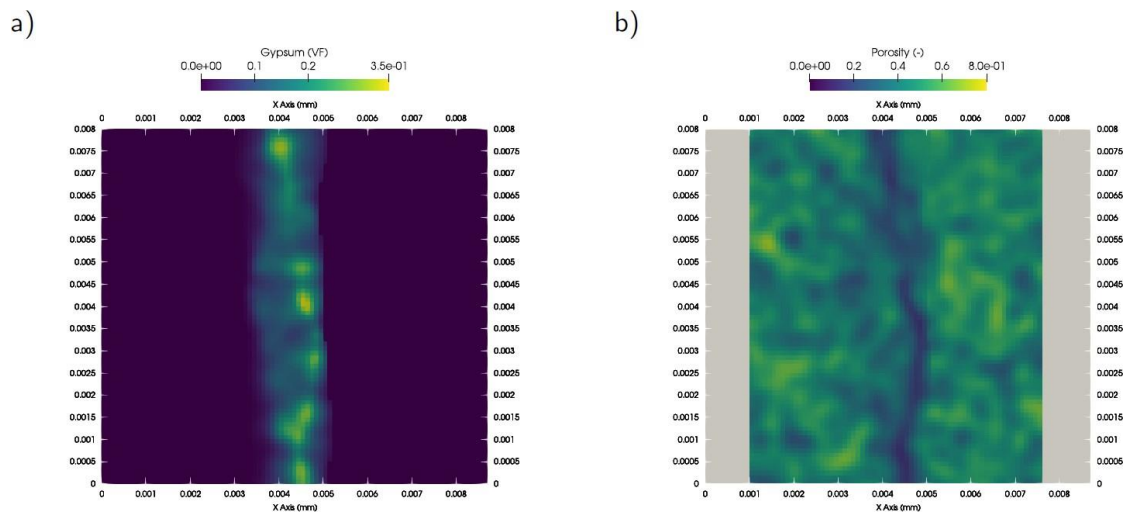
396 shows that presence of such reactive sites does not yield a final distribution of gypsum  
397 precipitation that is comparable to experimental results (see figure S4 in **supporting**  
398 **information**). Indeed, the location of nucleation control depends on where supersaturation is  
399 reached, which does not depend on reactivity. As further precipitation is dominated by the  
400 growth of gypsum, the precipitation front is very similar to the one observed for 1D  
401 simulations. Also, a purely random porosity field does not yield strong differences, as the  
402 lack of structure averages out the different path and yield a similar precipitation pattern (Fig  
403 4b).



404

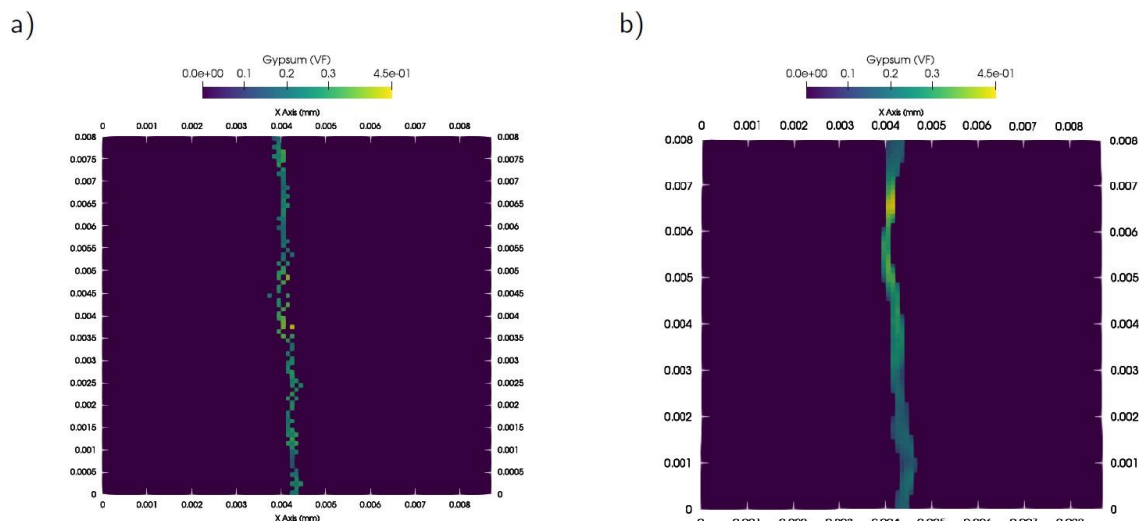
405 Figure 4: Distribution of Gypsum precipitation for two scenarios at the end of simulation time of 140  
406 days. a) Homogeneous porosity with varying reactivity of the porous medium. b) Purely random  
407 porosity field.

408 Conversely, using a porosity distribution exhibiting a certain degree of structure allows some  
409 locations to initiate precipitation before others and thereby leading to formation of a  
410 discontinuous zone of precipitation with certain clusters. The numerical simulation did show  
411 such behavior on formation of isolated clusters of gypsum (Fig. 5 a) and which is in very  
412 good visual agreement with tomographic images that are presented in figure S4 in  
413 **supporting information**. Based on these simulations, it seems that the appearance of  
414 clusters is dependent on the combined effect of relative rates of transport and reaction  
415 kinetics. Furthermore, the influence of nucleation kinetics on gypsum precipitation is  
416 illustrated in Figure-6. Figure-6a shows that nucleation driven kinetics leads to discrete spots  
417 of precipitation, while Figure-6b shows that growth-driven kinetics yields thin precipitation  
418 zone.



419419

420 Figure 5: Final distribution of gypsum and associated porosity reduction for 2D simulations. Porosity  
 421 of the reservoirs (above 1) is excluded from the color scale.



422422

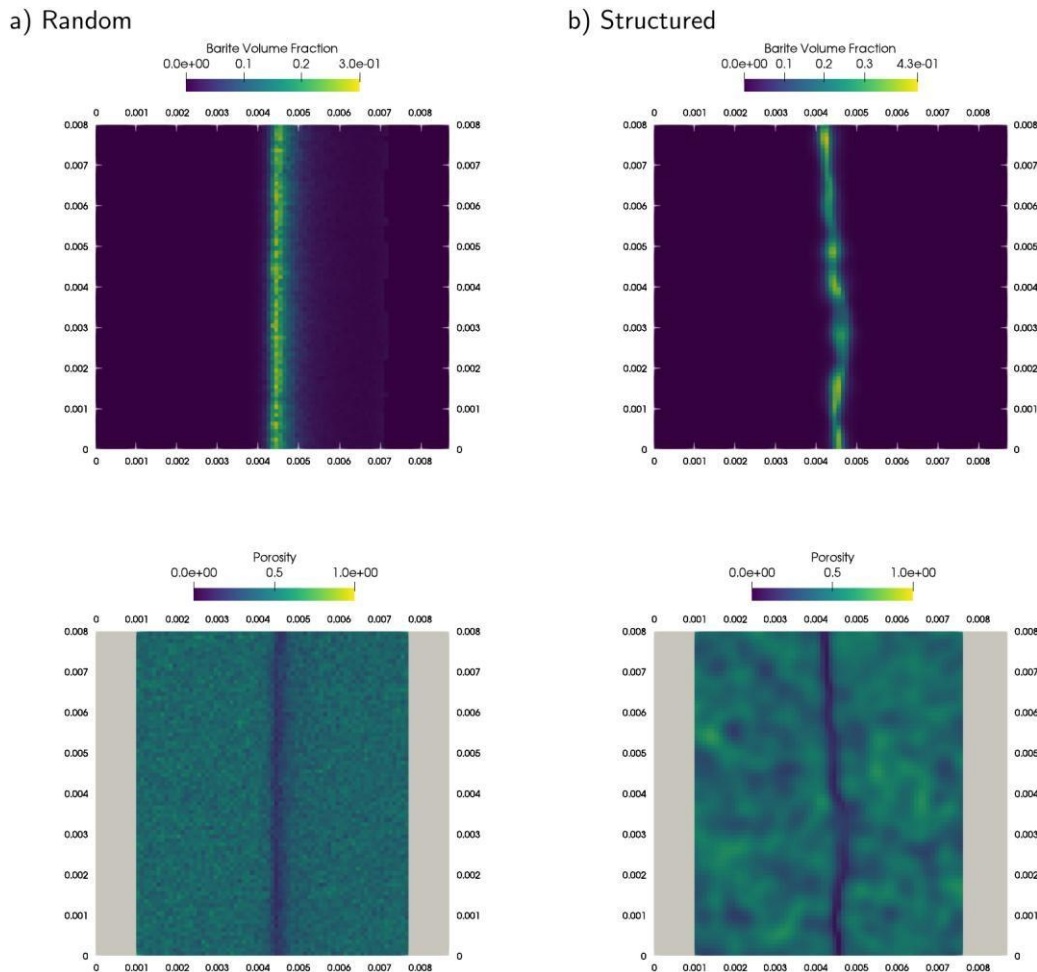
423 Figure 6: Influence of the nucleation mode. A) Nucleation driven precipitation modelled by a high  
 424 initial porous medium reactivity. B) Gypsum-growth mechanism. One must note that the presented  
 425 precipitation patterns were obtained at the end of simulation time of 140 days

426426

### 427 3.3 Barite simulation with spatial variability

428 We have shown that, for the gypsum case, incorporating a structured porosity field was  
 429 required. One may wonder as what are the impacts of considering these pore-scale  
 430 heterogeneities for the barite simulation. The results presented in Figure 7, shows a cross-  
 431 section view of 2D barite simulation carried out in the two random heterogeneous porosity  
 432 fields (with and without structure). In both cases, barite precipitation is confined within a thin  
 433 zone in the center of the sample. Simulation suggests a significant porosity loss within the  
 434 clogged zone in the porous medium at the end of the experiment (Figure 7). Both  
 435 simulations display similar formation of a thin, continuous and regular, barite-clogged area.  
 436 Comparison of both simulations confirms that for the barite experiment, spatial variability

437 triggers small local variations in the diffusion of reactants towards the center of the sample;  
438 however, due to the low solubility of barite, the supersaturation to initiate precipitation is  
439 similar to the (1D) homogeneous base case. The slow kinetics further compensated the  
440 impact of local variation in selective precipitation initiation preventing the scenario of spheres  
441 formation. As simulations proceeds, barite grows at these first points of precipitates in the  
442 center of the sample. Nevertheless, one could clearly observe that the clogged zone  
443 formation using of structured porosity field produce barite distributions closer to experimental  
444 results (refer to Figure S5 in Supporting information).



445445

446 Figure 7: evolution of barite volume fraction (top) and porosity field (bottom) mineral using HYTEC  
447 at the end of the simulation (140 days).

448448

#### 449 4 Conclusion:

450 In this study, two sets of numerical simulations were performed to investigate coupled impact  
451 of physical properties in the form of pore structure heterogeneity with chemical properties in  
452 the form of mineral intrinsic properties (solubility, rate kinetics) in driving distribution and  
453 porosity loss via secondary mineral formation. The 1D modeling results derived crucial  
454 information on location of clogged area, total porosity loss and mass transfer from inlet

455 reservoirs to sample. For barite precipitation in chalk, the experiments showed the formation  
456 of clogging zone a thin layered structure and was located at the center of the sample. At 1D,  
457 it was possible to reproduce this clogging feature using numerical simulations and with  
458 correct estimation of  $Ba^{2+}$  and  $SO_4^{2-}$  diffusion from sample boundary, overall amount of  
459 barite precipitation in the sample, and fair estimation of feedback on water tracer diffusivity.  
460 Thus, these simulations show that for some mineral such as barite, 1D simulations are  
461 useful to derive the processes at boundary conditions. For gypsum experiments, the  
462 numerical simulations fairly determined the  $Ca^{2+}$  and  $SO_4^{2-}$  diffusion from sample boundary.  
463 The simulations also correctly hinted towards diffusion of ions into the counter reservoirs and  
464 contributing to precipitation at bulk conditions. However, in this case Archie's relationship  
465 clearly underestimated the tracer transport after formation of clogging zone. Nevertheless,  
466 both barite and gypsum experiments clearly hinted towards performing numerical  
467 simulations where clogging behavior could be modeled by taking into account the presence  
468 of small-scale structured heterogeneities that could not be resolved in 1D via sensitivity  
469 analysis by changing parameters such kinetic rate, cementation factor, mesh size and  
470 saturation index values. In this view, the first set of numerical simulations at 2D scale  
471 considered investigating precipitates distribution and local porosity loss in response to  
472 structured and unstructured random porosity fields. However, the second set of numerical  
473 simulations considered investigating the formation of clogging zone in a chalk sample that  
474 initially contains randomly sprayed reactive surfaces. In the former case, the aim of  
475 simulations was to investigate the competition between mass transport and reaction kinetics,  
476 and in latter case, the aim of simulations was to generate a competition between kinetic  
477 driven and nucleation growth precipitation. The results of both simulations exercise showed  
478 that the consideration of structured heterogeneous porosity field showed gypsum distribution  
479 very similar to experimental results. These findings clearly validate the assumption  
480 presented in (Rajyaguru et al., 2019), *i.e.* "gypsum precipitation behavior in chalk is due to  
481 strong coupling between reaction kinetics and pore structure heterogeneity." However, the  
482 simulations results for barite conducted for purely random and structured porosity field  
483 showed a thin layered clogging front in the center of the sample. This observation clearly  
484 hints towards the fact that barite precipitation is indeed growth dependent. Thus, the  
485 numerical simulations presented in this study provide an essential information pertaining to  
486 the choice of scale that is necessary for studying clogging in porous media. A key  
487 information that could be derived from this exercise is the need to develop dedicated  
488 experimental datasets and test them using pore-scale modelling. It is imperative that the  
489 strong coupling of such experimental and numerical exercises could only derive the novel  
490 feedback relationship replacing Archie's relationship.

491 Finally, from 1D and 2D experimental results, we conclude that reactive transport  
492 simulations enabled to validate the model based on experimental results presented in  
493 (Rajyaguru et al., 2019), *i.e.* "how the physicochemical processes at stake yielded such  
494 different precipitation morphologies." In the end, the understanding obtained by the reactive  
495 transport approach allows to draw conclusions that may be suited to other types of  
496 simulations with geoengineering relevance.

497497

498498

499499

500500

501501

502502

503503

504504

505 References

- 506 Archie, G.E., 1942. The Electrical Resistivity Log as an Aid in Determining Some Reservoir  
507 Characteristics. *Trans. AIME* 146, 54-62. <https://doi.org/10.2118/942054-G>
- 508 Bear, J., 2013. *Dynamics of fluids in porous media*. Courier Corporation.
- 509 Berkowitz, B., Cortis, A., Dentz, M., Scher, H., 2006. Modeling Non-fickian transport in  
510 geological formations as a continuous time random walk. *Rev. Geophys.* 44, 1-49.  
511 <https://doi.org/10.1029/2005RG000178>
- 512 Berthe, G., 2012. Évolution des propriétés de confinement des roches-couvertures type  
513 argilite soumises à des fluides enrichis en CO<sub>2</sub>: impact des discontinuités naturelles et  
514 artificielles. Université Paris Sud-Paris XI. Français. NNT : 2012PA112420. tel-  
515 00795668.
- 516 Bradbury, M.H., Berner, U., Curti, E., Hummel, W., Kosakowski, G., Thoenen, T., 2014. The  
517 long term geochemical evolution of the nearfield of the HLW repository. Paul Scherrer  
518 Institute (PSI).
- 519 Bruns, S., Stipp, S.L.S., Sørensen, H.O., 2017. Statistical representative elementary  
520 volumes of porous media determined using greyscale analysis of 3D tomograms. *Adv.*  
521 *Water Resour.* 107, 32-42.
- 522 Carman, P.C., 1937. Fluid flow through granular beds. *Trans. Inst. Chem. Eng.* 15, 150-166.
- 523 Cochepin, B., Trotignon, L., Bildstein, O., Steefel, C.I., Lagneau, V., Van der lee, J., 2008.  
524 Approaches to modelling coupled flow and reaction in a 2D cementation experiment.  
525 *Adv. Water Resour.* 31, 1540-1551. <https://doi.org/10.1016/j.advwatres.2008.05.007>
- 526 Deng, H., Tournassat, C., Molins, S., Claret, F., Steefel, C.I., 2021. A Pore-Scale  
527 Investigation of Mineral Precipitation Driven Diffusivity Change at the Column-Scale.  
528 *Water Resour. Res.* 57, e2020WR028483.
- 529 Faÿ-Gomord, O., Soete, J., Davy, C.A., Janssens, N., Troadec, D., Cazaux, F., Caline, B.,  
530 Swennen, R., 2017. Tight chalk: Characterization of the 3D pore network by FIB-SEM,  
531 towards the understanding of fluid transport. *J. Pet. Sci. Eng.* 156, 67-74.  
532 <https://doi.org/10.1016/j.petrol.2017.05.005>
- 533 Glaus, M.A., Frick, S., Van Loon, L.R., 2020. A coherent approach for cation surface  
534 diffusion in clay minerals and cation sorption models: Diffusion of Cs<sup>+</sup> and Eu<sup>3+</sup> in  
535 compacted illite as case examples. *Geochim. Cosmochim. Acta* 274, 79-96.
- 536 Hjuler, M.L., Fabricius, I.L., 2009. Engineering properties of chalk related to diagenetic  
537 variations of Upper Cretaceous onshore and offshore chalk in the North Sea area. *J.*  
538 *Pet. Sci. Eng.* 68, 151-170. <https://doi.org/10.1016/j.petrol.2009.06.005>
- 539 Jun, Y.S., Giammar, D.E., Werth, C.J., 2013. Impacts of geochemical reactions on geologic  
540 carbon sequestration. *Environ. Sci. Technol.* 47, 3-8.  
541 <https://doi.org/10.1021/es3027133>
- 542 Kashchiev, D., van Rosmalen, G.M., 2003. Review: Nucleation in solutions revisited. *Cryst.*  
543 *Res. Technol.* 38, 555-574. <https://doi.org/10.1002/crat.200310070>
- 544 Lagneau, V., 2013. Modélisation des couplages entre réactions géochimiques et processus  
545 hydrodynamiques en milieu poreux - applications au stockage de CO<sub>2</sub> et à  
546 l'exploitation d'uranium. *Géochimie*. Université Pierre et Marie Curie - Paris VI, 2013.  
547 tel-00879817.

- 548 Lagneau, V., van der Lee, J., 2010. Operator-splitting-based reactive transport models in  
549 strong feedback of porosity change: The contribution of analytical solutions for accuracy  
550 validation and estimator improvement. *J. Contam. Hydrol.* 112, 118-129.  
551 <https://doi.org/10.1016/j.jconhyd.2009.11.005>
- 552 Landesman, C., Macé, N., Radwan, J., Ribet, S., Bessaguet, N., David, K., Page, J.,  
553 Henocq, P., 2018. Effect of high saline alkaline conditions onto radionuclide transport in  
554 a CEM V/A hardened cement paste, in: NUWCEM, Cement-Based Materials for  
555 Nuclear Waste.
- 556 Lasaga, A.C., 2014. Kinetic theory in the earth sciences. Princeton university press.
- 557 Moldovan, B.J., Jiang, D.T., Hendry, M.J., 2003. Mineralogical characterization of arsenic in  
558 uranium mine tailings precipitated from iron-rich hydrometallurgical solutions. *Environ.*  
559 *Sci. Technol.* 37, 873-879. <https://doi.org/10.1021/es025947a>
- 560 Müter, D., Sørensen, H.O., Jha, D., Harti, R., Dalby, K.N., Suhonen, H., Feidenhans'l, R.,  
561 Engstrøm, F., Stipp, S.L.S., 2014. Resolution dependence of petrophysical parameters  
562 derived from X-ray tomography of chalk. *Appl. Phys. Lett.* 105, 43108.
- 563 Nagaraja, B.M., Abimanyu, H., Jung, K.D., Yoo, K.S., 2007. Preparation of mesostructured  
564 barium sulfate with high surface area by dispersion method and its characterization. *J.*  
565 *Colloid Interface Sci.* 316, 645-651. <https://doi.org/10.1016/j.jcis.2007.09.004>
- 566 Noiriél, C., Seigneur, N., Le Guern, P., Lagneau, V., 2021. Geometry and mineral  
567 heterogeneity controls on precipitation in fractures: An X-ray micro-tomography and  
568 reactive transport modeling study. *Adv. Water Resour.* 152, 103916.
- 569 Nooraiepour, M., Masoudi, M., Hellevang, H., 2021. Probabilistic nucleation governs time,  
570 amount, and location of mineral precipitation and geometry evolution in the porous  
571 medium. *Sci. Rep.* 11, 1-17.
- 572 Potgieter, J.H., Strydom, C.A., 1996. An investigation into the correlation between different  
573 surface area determination techniques applied to various limestone-related compounds.  
574 *Cem. Concr. Res.* 26, 1613-1617. [https://doi.org/10.1016/S0008-8846\(96\)00159-7](https://doi.org/10.1016/S0008-8846(96)00159-7)
- 575 Prasianakis, N.I., Curti, E., Kosakowski, G., Poonosamy, J., Churakov, S. V., 2017.  
576 Deciphering pore-level precipitation mechanisms. *Sci. Rep.* 7, 1-9.  
577 <https://doi.org/10.1038/s41598-017-14142-0>
- 578 Prieto, M., 2014. Nucleation and supersaturation in porous media (revisited). *Mineral. Mag.*  
579 78, 1437-1447. <https://doi.org/10.1180/minmag.2014.078.6.11>
- 580 Rajyaguru, A., L'Hôpital, E., Savoye, S., Wittebroodt, C., Bildstein, O., Arnoux, P., Detilleux,  
581 V., Fatnassi, I., Gouze, P., Lagneau, V., 2019. Experimental characterization of coupled  
582 diffusion reaction mechanisms in low permeability chalk. *Chem. Geol.* 503.  
583 <https://doi.org/10.1016/j.chemgeo.2018.10.016>
- 584 Renard, D., Bez, N., Desassis, N., Beucher, H., Ors, F., Laporte, F., 2015. RGeostats: The  
585 Geostatistical package [version: 11.0. 3]. MINES ParisTech. Free download from  
586 <http://cg.ensmp.fr/rgeostats>.
- 587 Røgen, B., Fabricius, I.L., 2002. Influence of clay and silica on permeability and capillary  
588 entry pressure of chalk reservoirs in the North Sea. *Pet. Geosci.* 8, 287-293.
- 589 Sabo, M.S., Beckingham, L.E., 2021. Porosity-Permeability Evolution During Simultaneous  
590 Mineral Dissolution and Precipitation. *Water Resour. Res.* 57, e2020WR029072.

591 Seigneur, N., Mayer, K.U., Steefel, C.I., 2019. Reactive transport in evolving porous media.  
592 *Rev. Mineral. Geochemistry* 85, 197-238.

593 Snæbjörnsdóttir, S.Ó., Sigfússon, B., Marieni, C., Goldberg, D., Gislason, S.R., Oelkers,  
594 E.H., 2020. Carbon dioxide storage through mineral carbonation. *Nat. Rev. Earth*  
595 *Environ.* 1, 90-102.

596 Steefel, C.I., Yang, L., 2021. Secondary magnesite formation from forsterite under CO<sub>2</sub>  
597 sequestration conditions via coupled heterogeneous nucleation and crystal growth.  
598 *Geochim. Cosmochim. Acta* 311, 29-42.

599 Steinwinder, J., Beckingham, L.E., 2019. Role of pore and pore-throat distributions in  
600 controlling permeability in heterogeneous mineral dissolution and precipitation  
601 scenarios. *Water Resour. Res.* 55, 5502-5517.

602 Thakur, J.K., Thakur, R.K., Ramanathan, A.L., Kumar, M., Singh, S.K., 2010. Arsenic  
603 contamination of groundwater in Nepal—an overview. *Water* 3, 1-20.

604 Trincherò, P., Iraola, A., 2020. Models for the assessment of transport of naturally-occurring  
605 nuclides in fractured media. *J. Hydrol.* 580, 124322.

606 van der Lee, J., De Windt, L., Lagneau, V., Goblet, P., 2003. Module-oriented modeling of  
607 reactive transport with HYTEC. *Comput. Geosci.* 29, 265-275.  
608 [https://doi.org/10.1016/S0098-3004\(03\)00004-9](https://doi.org/10.1016/S0098-3004(03)00004-9)

609 Varzina, A., Cizer, Ö., Yu, L., Liu, S., Jacques, D., Perko, J., 2020. A new concept for pore-  
610 scale precipitation-dissolution modelling in a lattice Boltzmann framework-Application  
611 to portlandite carbonation. *Appl. Geochemistry* 123, 104786.

612 Villanova, J., Laurencin, J., Cloetens, P., Bleuet, P., Delette, G., Suhonen, H., Usseglio-  
613 Viretta, F., 2013. 3D phase mapping of solid oxide fuel cell YSZ/Ni cermet at the  
614 nanoscale by holographic X-ray nanotomography. *J. Power Sources* 243, 841-849.

615 Yoon, H., Dewers, T.A., 2013. Nanopore structures, statistically representative elementary  
616 volumes, and transport properties of chalk. *Geophys. Res. Lett.* 40, 4294-4298.

617 Zhang, J., Nancollas, G.H., 1992. Influence of calcium/sulfate molar ratio on the growth rate  
618 of calcium sulfate dihydrate at constant supersaturation. *J. Cryst. Growth* 118, 287-  
619 294. [https://doi.org/10.1016/0022-0248\(92\)90073-R](https://doi.org/10.1016/0022-0248(92)90073-R)

620